Supplementary Information of Boreal Env. Res. Vol. 31: 45–62, 2026

Supplementary Information of

Profound analysis of sulfuric acid proxies at a boreal forest site in southern Finland

***Jaakkola et al*.**

Correspondence to: Ilona Jaakkola (ilona.a.jaakkola@helsinki.fi)

Solved forms of sulfuric acid proxies (Eqs. 1–4):

Proxy 1:

$$[\mathrm{H_2SO_4}]_{\mathrm{proxy}} = -\frac{\mathrm{CS}}{2k_{\mathrm{DIM}}} + \sqrt{\left(\frac{\mathrm{CS}}{2k_{\mathrm{DIM}}}\right)^2 + \frac{[\mathrm{SO_2}]}{k_{\mathrm{DIM}}}\left(k_{\mathrm{RAD}}\,\mathrm{RAD} + k_{\mathrm{sCI}}[\mathrm{O_3}][\mathrm{MT}]\right)} \quad \text{(S1)}$$

Proxy 2:

$$[\mathrm{H_2SO_4}]_{\mathrm{proxy}} = -\frac{\mathrm{CS}}{2k_{\mathrm{DIM}}} + \sqrt{\left(\frac{\mathrm{CS}}{2k_{\mathrm{DIM}}}\right)^2 + \frac{[\mathrm{SO_2}]}{k_{\mathrm{DIM}}}k_{\mathrm{RAD}}\mathrm{RAD}} \quad \text{(S2)}$$

Proxy 3:

$$[\mathrm{H_2SO_4}]_{\mathrm{proxy}} = \frac{[\mathrm{SO_2}]}{\mathrm{CS}}\left(k_{\mathrm{RAD}}\mathrm{RAD} + k_{\mathrm{sCI}}[\mathrm{O_3}][\mathrm{MT}]\right) \quad \text{(S3)}$$

Proxy 4:

$$[\mathrm{H_2SO_4}]_{\mathrm{proxy}} = \frac{[\mathrm{SO_2}]}{\mathrm{CS}}k_{\mathrm{RAD}}\mathrm{RAD} \quad \text{(S4)}$$

Proxy 5:

$$[\mathrm{H_2SO_4}]_{\mathrm{proxy}} = -\frac{k_{\mathrm{CS}}\mathrm{CS}}{2k_{\mathrm{DIM}}} + \sqrt{\left(\frac{k_{\mathrm{CS}}CS}{2k_{\mathrm{DIM}}}\right)^2 + \frac{[\mathrm{SO_2}]}{k_{\mathrm{DIM}}}\left(k_{\mathrm{RAD}}\mathrm{RAD} + k_{\mathrm{sCI}}[\mathrm{O_3}][\mathrm{MT}]\right)}. \quad \text{(S5)}$$

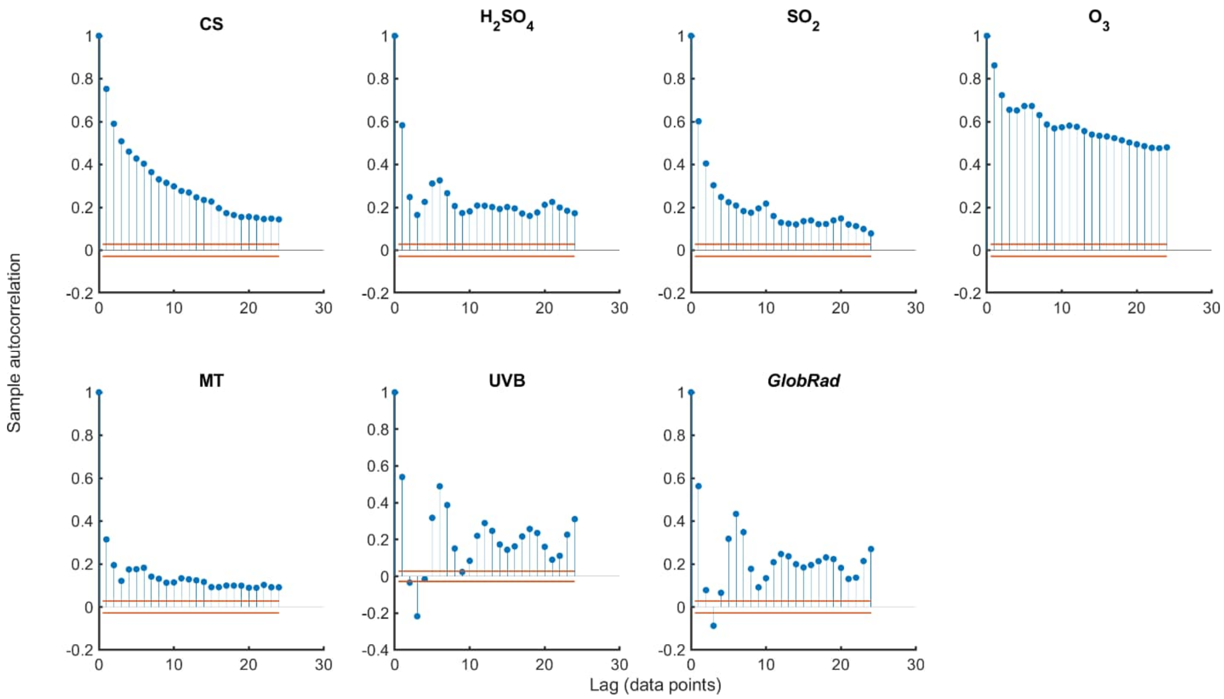

Figure S1: Autocorrelation in the measured predictor variables of the proxies. Autocorrelation is calculated with the *autocorr* function of MATLAB.

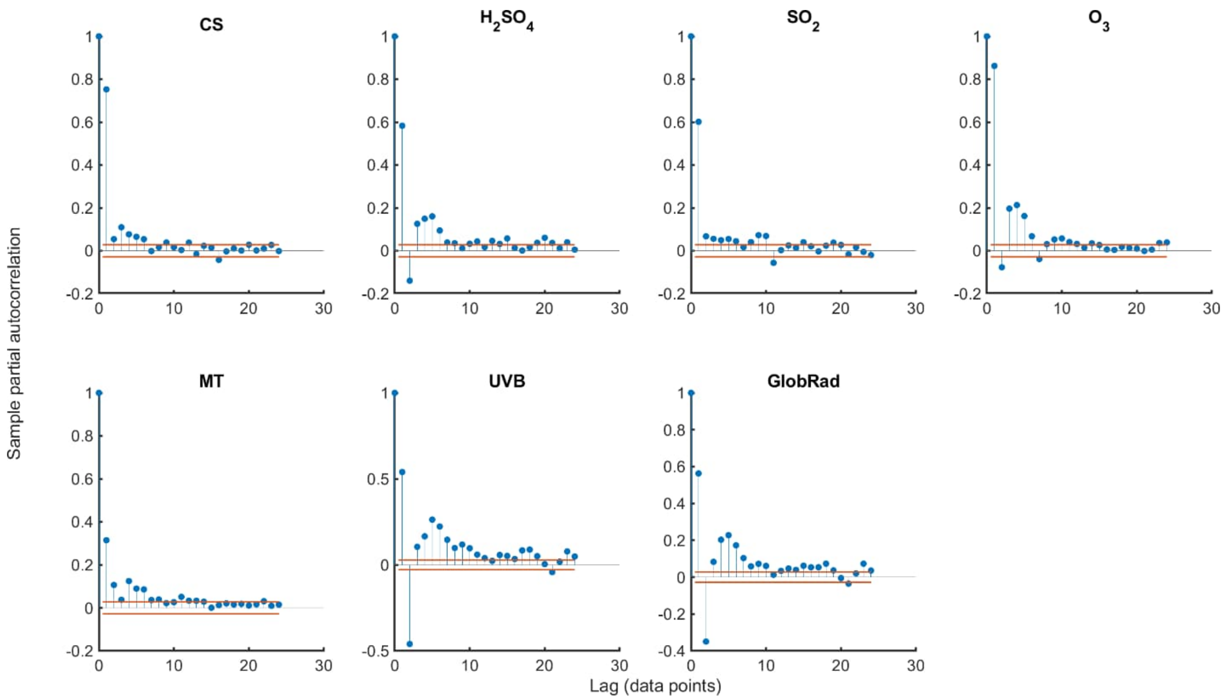

Figure S2: Partial autocorrelation in the measured predictor variables of the proxies. Partial autocorrelation is calculated with the *parcorr* function of MATLAB.

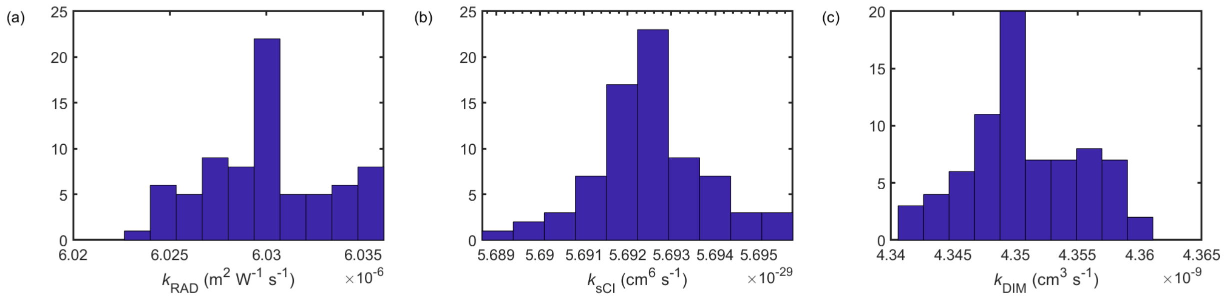

Figure S3: Distribution of fitting coefficients from 75 fits associated with the lowest loss function values among the 100 refits for proxy 1 with UVB radiation.

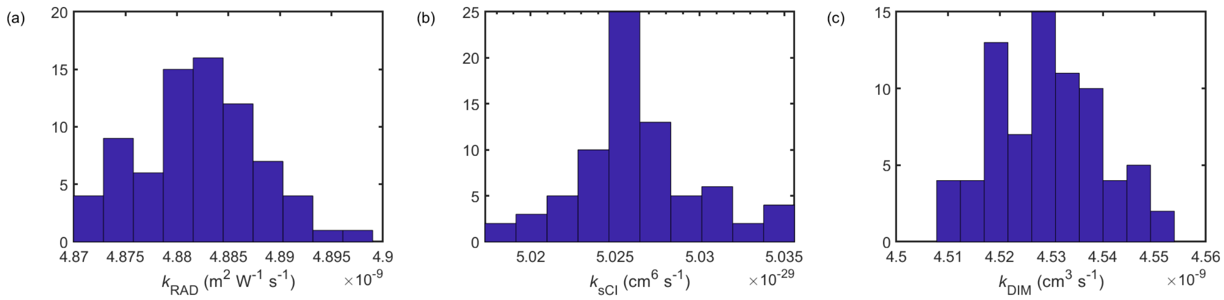

Figure S4: Distribution of fitting coefficients from 75 fits associated with the lowest loss function values among the 100 refits for proxy 1 with global radiation.

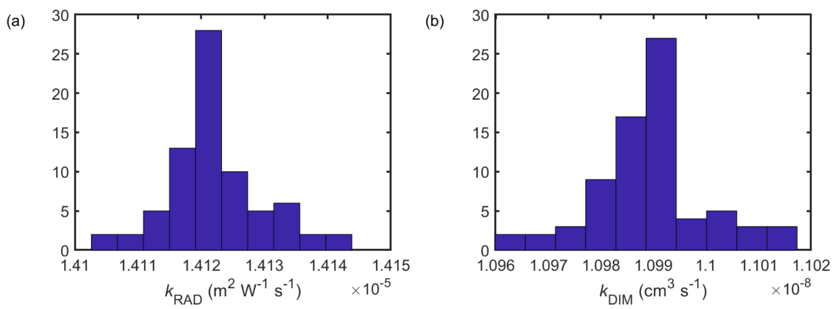

Figure S5: Distribution of fitting coefficients from 75 fits associated with the lowest loss function values among the 100 refits for proxy 2 with UVB radiation.

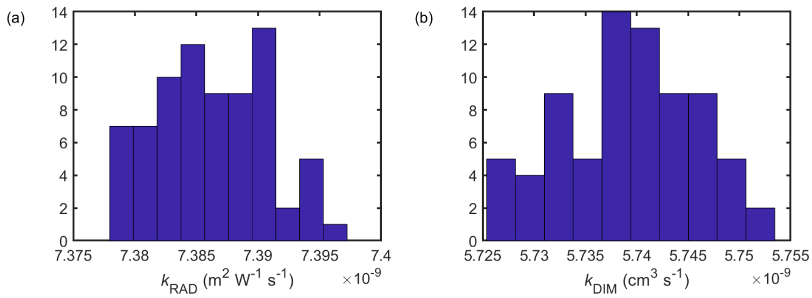

Figure S6: Distribution of fitting coefficients from 75 fits associated with the lowest loss function values among the 100 refits for proxy 2 with global radiation.

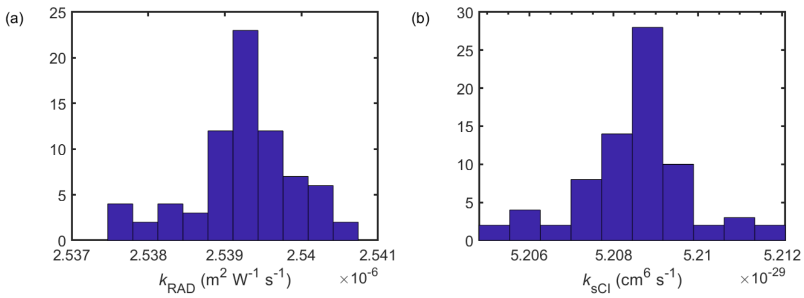

Figure S7: Distribution of fitting coefficients from 75 fits associated with the lowest loss function values among the 100 refits for proxy 3 with UVB radiation.

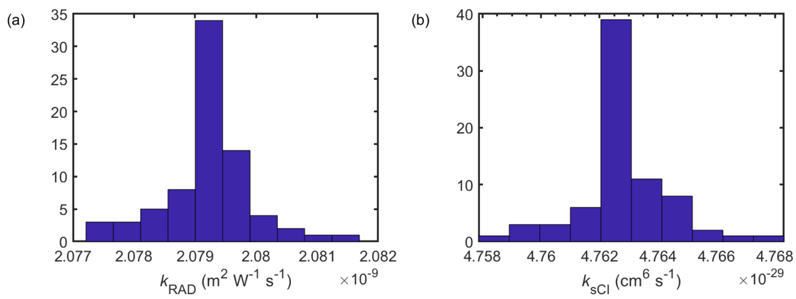

Figure S8: Distribution of fitting coefficients from 75 fits associated with the lowest loss function values among the 100 refits for proxy 3 with global radiation.

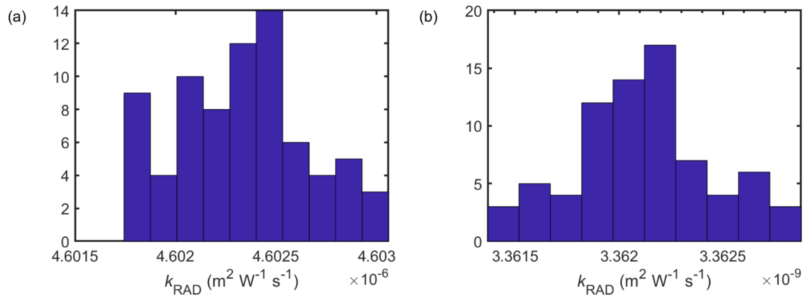

Figure S9: Distribution of fitting coefficients from 75 fits associated with the lowest loss function values among the 100 refits for proxy 4 with (a) UVB and (b) global radiation.

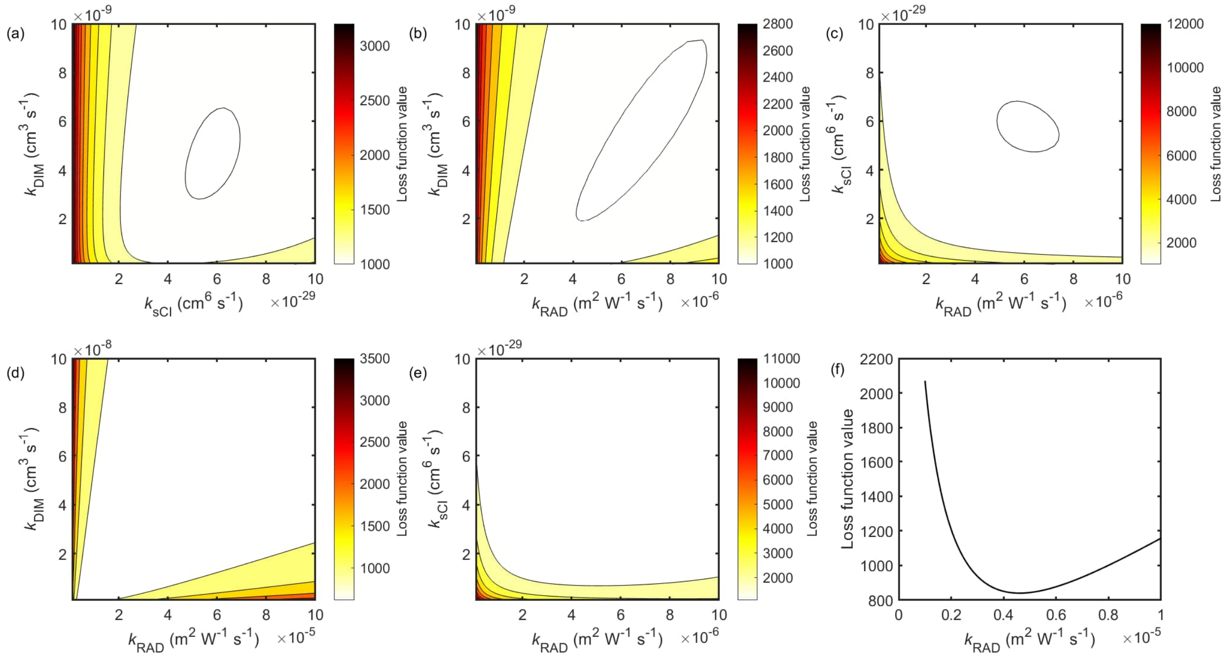

Figure S10: Surface plots of the minimized fitting function (sum of squared logarithm of the ratio between proxy values and measured sulfuric acid concentration; color) in relation to fitting coefficient values for UVB radiation-derived proxies: (a)–(c) proxy 1, (d) proxy 2, (e) proxy 3, and (f) proxy 4. For proxy 1, one of the fitting coefficients was held constant (value given by Table 1) in order to vary the two other coefficients. In (a) k_{RAD} was constant, in (b) k_{sCI}, and in (c) k_{DIM}.

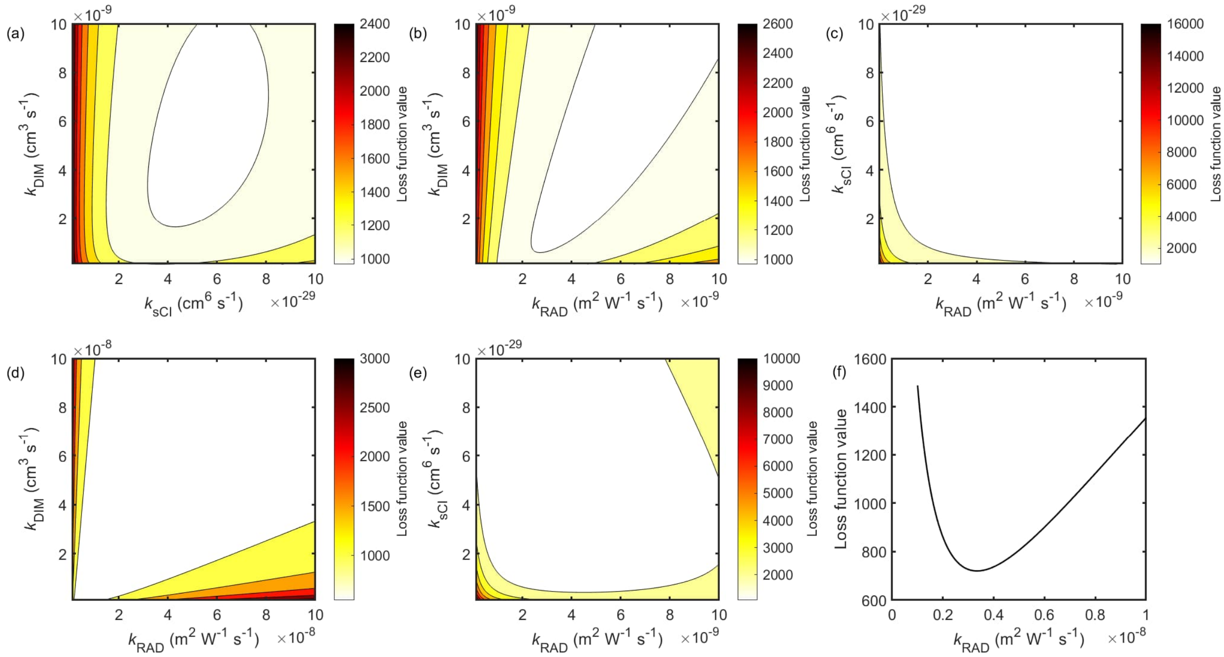

Figure S11: Surface plots of the minimized fitting function (sum of squared logarithm of the ratio between proxy values and measured sulfuric acid concentration; color) in relation to fitting coefficient values for global radiation derived proxies: (a)–(c) proxy 1, (d) proxy 2, (e) proxy 3, and (f) proxy 4. For proxy 1, one of the fitting coefficients was held constant (value given by Table 1) in order to vary the two other coefficients. In (a) k_{RAD} was constant, in (b) k_{sCI}, and in (c) k_{DIM}.

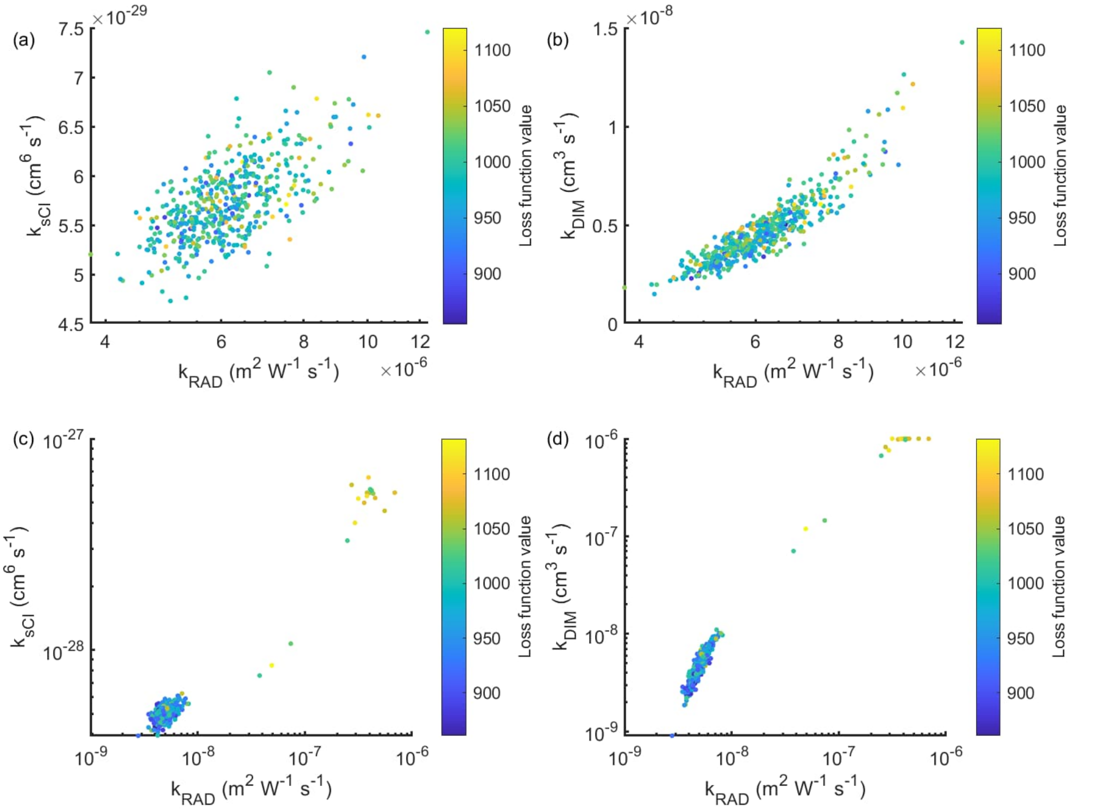

Figure S12: Fitting coefficients from 500 block bootstrap resamples colored with the loss function values for proxy 1 using the training dataset. (a) and (b) derived with UVB radiation, and (c) and (d) with global radiation.

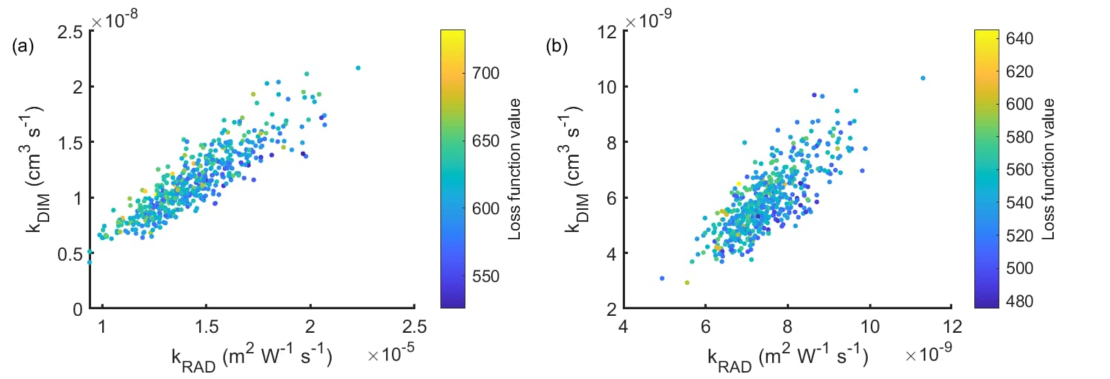

Figure S13: Fitting coefficients from 500 block bootstrap resamples colored with the loss function values for proxy 2 using the training dataset. (a) derived with UVB radiation and (b) with global radiation.

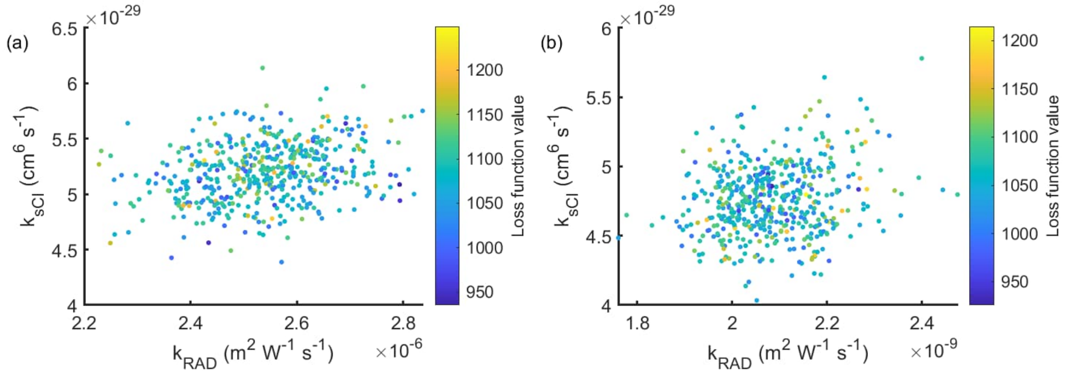

Figure S14: Fitting coefficients from 500 block bootstrap resamples colored with the loss function values for proxy 3 using the training dataset. (a) derived with UVB radiation and (b) with global radiation.

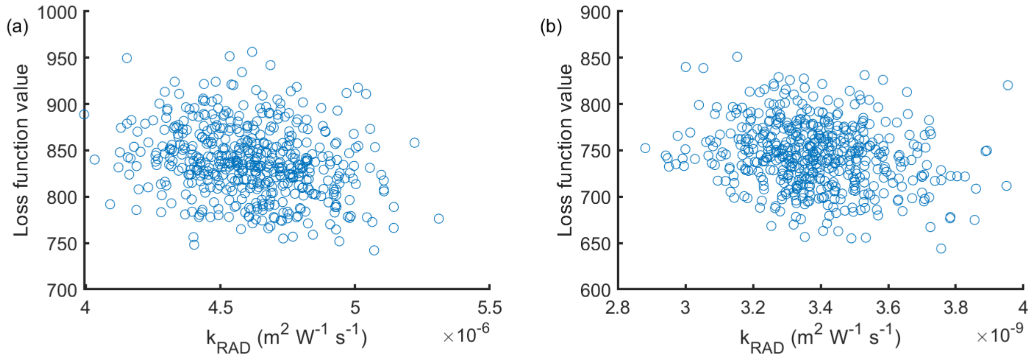

Figure S15: Fitting coefficients from 500 block bootstrap resamples colored with the loss function values for proxy 4 using the training dataset. (a) derived with UVB radiation and (b) with global radiation.

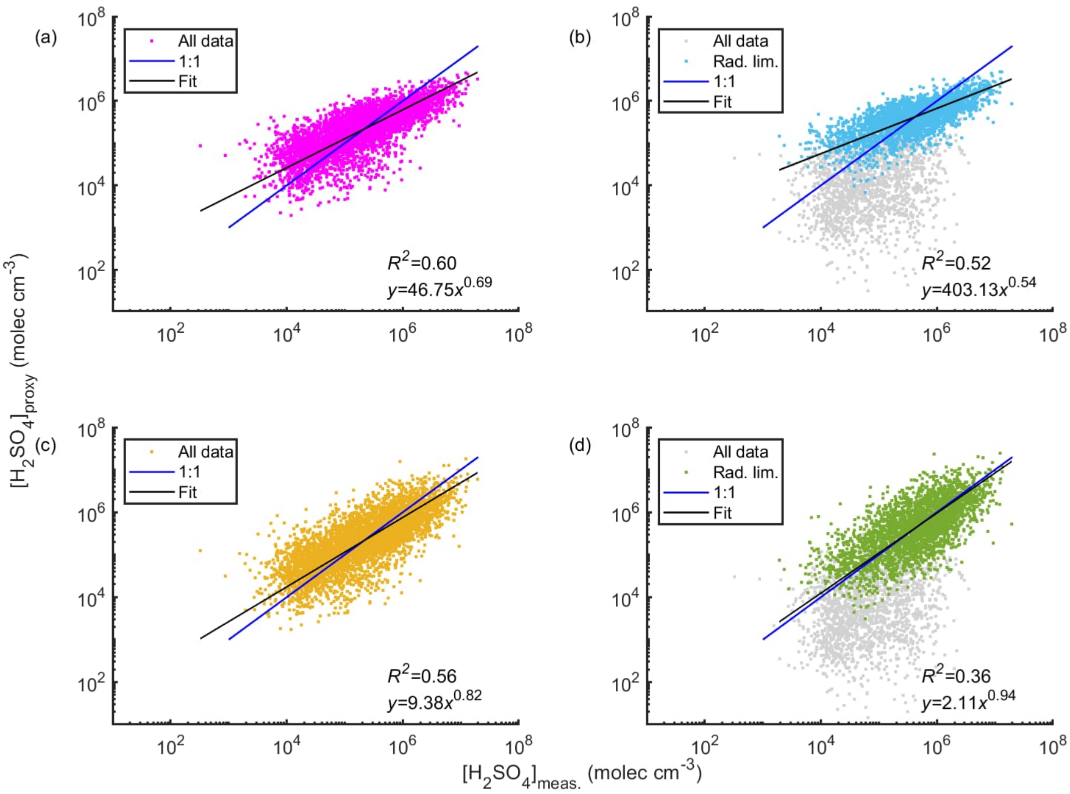

Figure S16: Sulfuric acid proxies using global radiation. (a) proxy 1, (b) proxy 2, (c) proxy 3, and (d) proxy 4. We applied radiation limits to proxies 2 and 4 (colored markers). Without radiation limits (gray markers), the R^2 values were -0.13 and -0.64, and the fitted lines were $y=2\cdot10^{-3}x^{1.47}$ and $y=7\cdot10^{-6}x^{1.89}$ for proxy 2 and proxy 4, respectively (fitted lines for all data not shown).

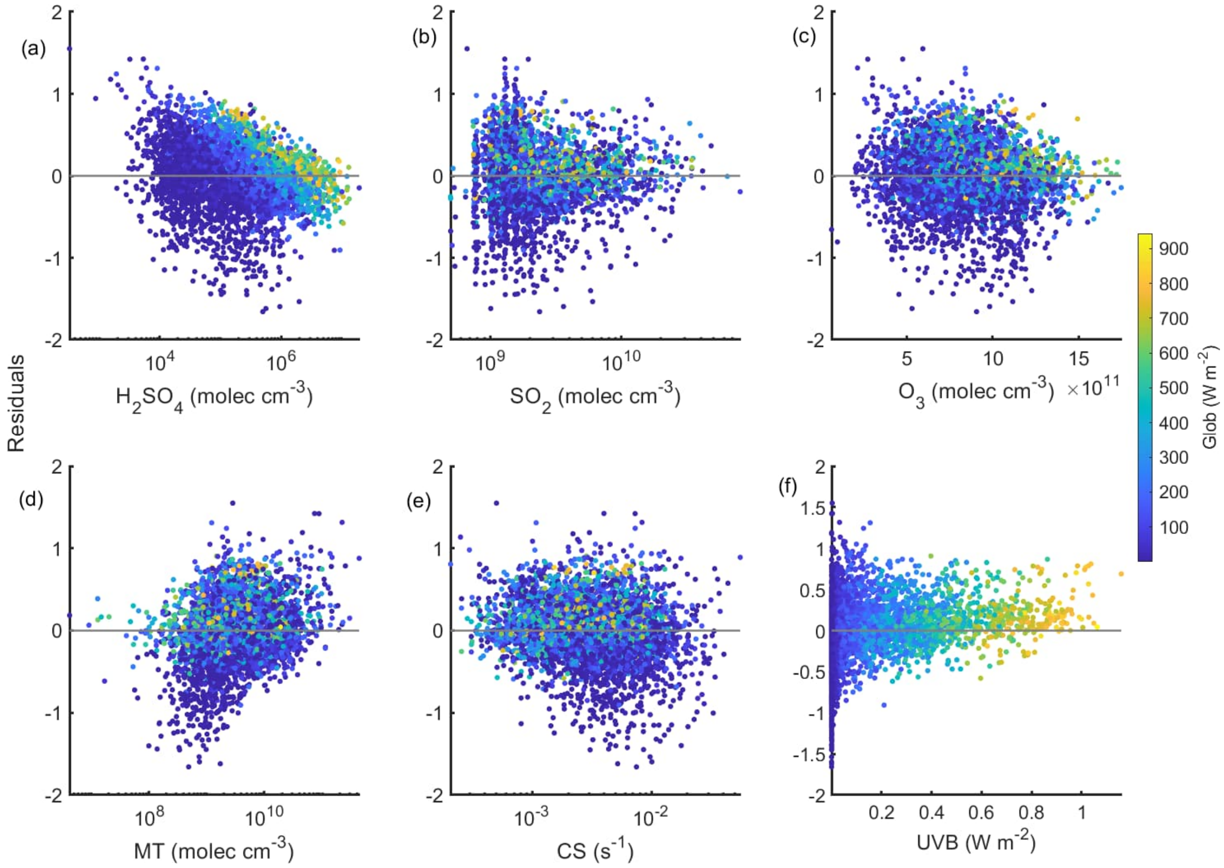

Figure S17: Residuals as a function of utilized fitting parameters for proxy 1 derived with UVB radiation.

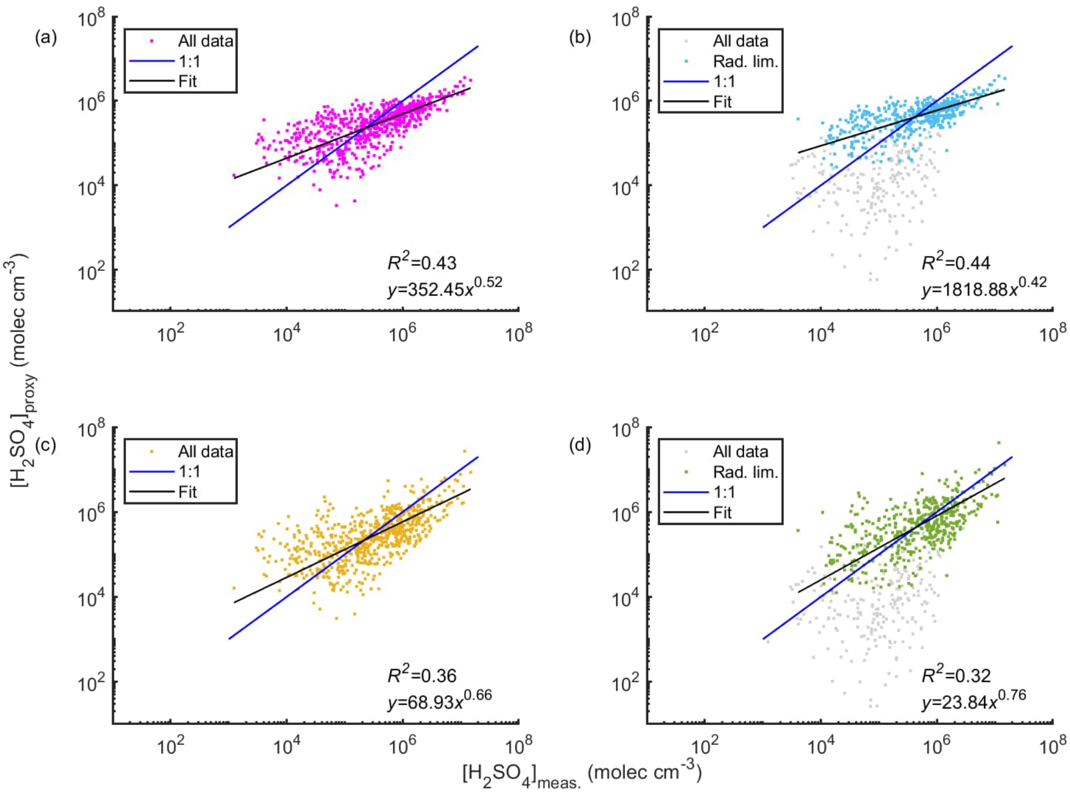

Figure S18: Sulfuric acid proxies with test dataset using global radiation. (a) proxy 1, (b) proxy 2, (c) proxy 3, and (d) proxy 4. We applied radiation limits for proxies 2 and 4 (colored markers). Without the radiation limits (gray markers), the R^2 values were -0.21 and -0.66, and the fitted lines were y=7·10^{-3}$x^{1.34}$ and y=1·10^{-5}$x^{1.85}$ for proxy 2 and proxy 4, respectively (fitted lines for all data not shown).

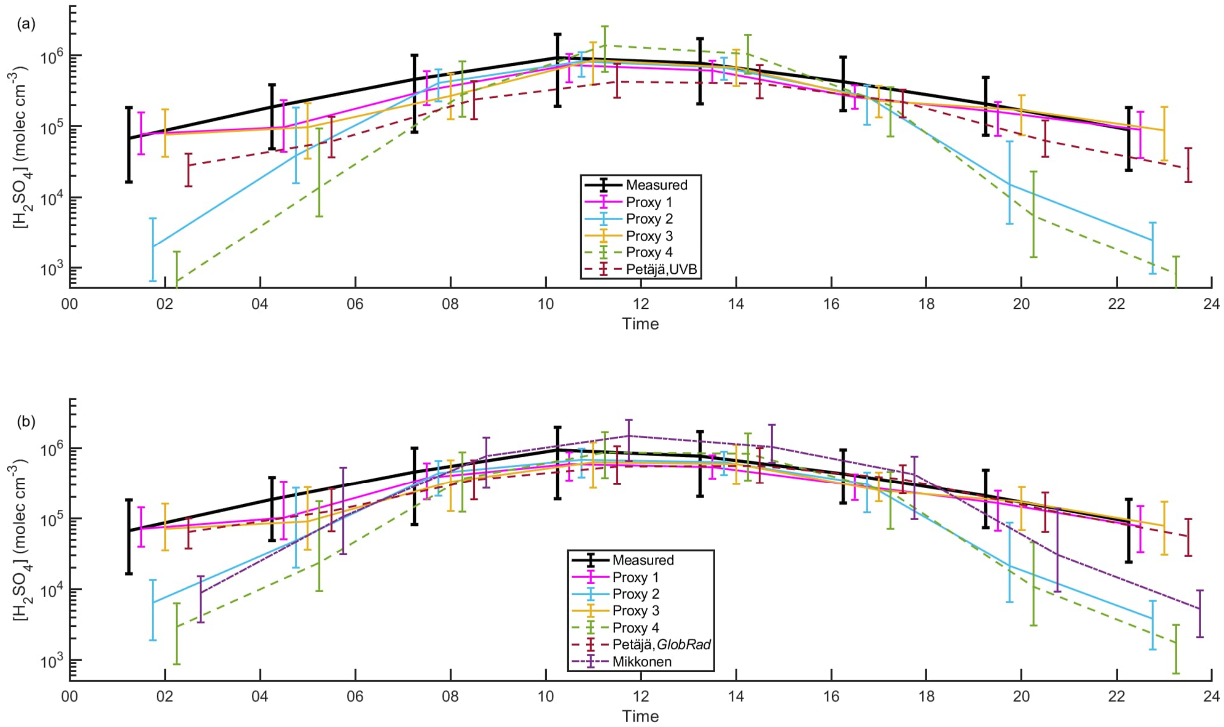

Figure S19: Hourly-averaged diurnal variation in sulfuric acid concentration in the test dataset, applying different proxies with (a) UVB and (b) global radiation. Bars indicate the 25th and 75th percentiles of the data. Petäjä refers to the sulfuric acid proxy by Petäjä et al. (2009), and Mikkonen to the sulfuric acid proxy by Mikkonen et al. (2011). Notice that due to the time resolution of monoterpene measurements, we have data points only every third hour.

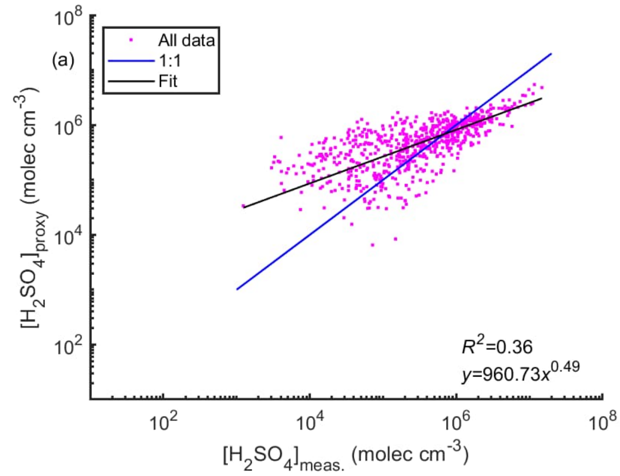

Figure S20: Sulfuric acid proxy corrected for hygroscopic growth by Dada et al. (2020) using the test dataset.

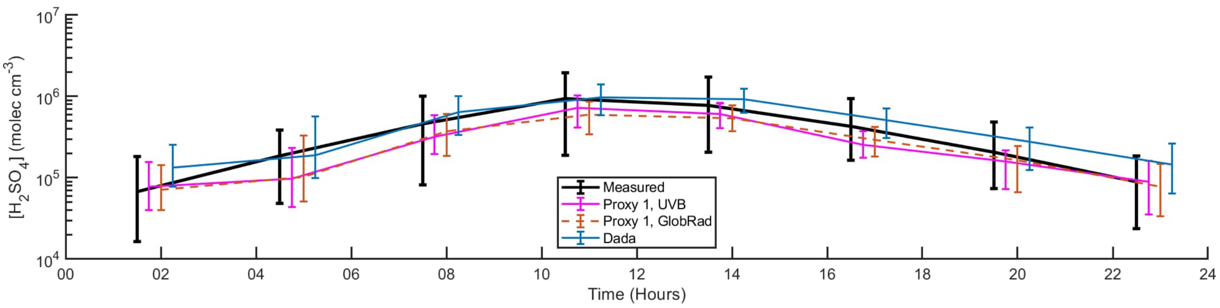

Figure S21: Hourly-averaged diurnal variation of sulfuric acid concentration of the test dataset, using proxy 1 with UVB and global radiation, as well as the proxy corrected for hygroscopic growth by Dada et al. (2020). For further details, see Fig. S19.

Table S1: Performance metrics of the test dataset. $\mathrm{SEM}/\sigma^2_{\mathrm{H_2SO}_{2,\mathrm{meas}}}$ is standard error of mean (SEM) of mean squared error (MSE) of each proxy across the 12 test data segments, divided by variance of the measured sulfuric acid concentration ($\sigma^2_{\mathrm{H_2SO}_{2,\mathrm{meas}}}$). The MSE (25th–75th) column shows the median MSE for each proxy across the test dataset segments, with the 25th and 75th percentiles in parenthesis. For proxies 2 and 4, values without the radiation limit are presented after the slash.

		$\mathrm{SEM}/\sigma^2_{\mathrm{H_2SO}_{2,\mathrm{meas}}}$	MSE (25th–75th)
UVB	Proxy 1	0.09	0.24 (0.13–0.42)
	Proxy 2	0.08 / 0.09	0.25 (0.15–0.31) / 0.88 (0.62–0.94)
	Proxy 3	0.12	0.23 (0.12–0.50)
	Proxy 4	0.10 / 0.14	0.30 (0.21–0.35) / 1.22 (0.99–1.44)
GlobRad	Proxy 1	0.09	0.22 (0.11–0.40)
	Proxy 2	0.07 / 0.11	0.22 (0.09–0.29) / 0.50 (0.46–0.68)
	Proxy 3	0.11	0.22 (0.12–0.45)
	Proxy 4	0.08 / 0.15	0.25 (0.16–0.34) / 0.72 (0.58–0.94)

Table S2: Pairwise comparison of performance of the proxies, based on MSE, across the 12 test data segments for (a) UVB and (b) global radiation. Each entry is read from row to column and indicates how many of the 12 segments the row proxy performed better (i.e., had lower MSE) than the column proxy. For proxies 2 and 4, values before the slash correspond to the version with the radiation limit, and values after the slash correspond to the version without the radiation limit.

(a)	Proxy 2	Proxy 3	Proxy 4	(b)	Proxy 2	Proxy 3	Proxy 4
Proxy 1	7 / 11	6	8 / 12	Proxy 1	3 / 10	8	7 / 10
Proxy 2		5 / 1	9 / 12	Proxy 2		7 / 1	8 / 11
Proxy 3			9 / 11	Proxy 3			7 / 11

Table S3: Fitting coefficients and coefficients of determination (R^2) of different proxies (Eqs. 1–4) for data fitted seasonally, using both UVB and global radiation. Values for proxies 2 and 4 are determined using the radiation limit.

		k_{RAD} (m^2 W^{-1} s^{-1})	k_{SCI} ($\cdot 10^{-29}$ cm^6 s^{-1})	k_{DIM} ($\cdot 10^{-9}$ cm^3 s^{-1})	R^2
P1, UVB	Spring	$5.053 \cdot 10^{-6}$	8.803	1.498	0.53
	Summer	$4.511 \cdot 10^{-6}$	6.410	4.441	0.48
	Autumn	$19.72 \cdot 10^{-6}$	5.670	8.076	0.56
	Winter	$34.72 \cdot 10^{-6}$	10.50	78.77	0.54
P2, UVB	Spring	$10.15 \cdot 10^{-6}$	–	3.251	0.51
	Summer	$65.93 \cdot 10^{-6}$	–	0.100	0.33
	Autumn	$8.807 \cdot 10^{-6}$	–	16.44	0.41
	Winter	$5.838 \cdot 10^{-6}$	–	1.130	0.60
P3, UVB	Spring	$2.750 \cdot 10^{-6}$	8.244	–	0.49
	Summer	$1.902 \cdot 10^{-6}$	6.101	–	0.45
	Autumn	$1.997 \cdot 10^{-6}$	2.976	–	0.45
	Winter	$3.153 \cdot 10^{-6}$	4.741	–	0.45
P4, UVB	Spring	$4.808 \cdot 10^{-6}$	–	–	0.37
	Summer	$5.415 \cdot 10^{-6}$	–	–	-0.26
	Autumn	$3.132 \cdot 10^{-6}$	–	–	0.17
	Winter	$3.132 \cdot 10^{-6}$	–	–	0.52
P1, *GlobRad*	Spring	$4.025 \cdot 10^{-9}$	8.274	1.778	0.53
	Summer	$4.682 \cdot 10^{-9}$	5.467	4.817	0.49
	Autumn	$12.69 \cdot 10^{-9}$	3.904	60.73	0.59
	Winter	$14.74 \cdot 10^{-9}$	8.242	58.32	0.57
P2, *GlobRad*	Spring	$6.478 \cdot 10^{-9}$	–	2.586	0.55
	Summer	$18.03 \cdot 10^{-9}$	–	27.64	0.39
	Autumn	$6.341 \cdot 10^{-9}$	–	14.41	0.46
	Winter	$3.647 \cdot 10^{-9}$	–	1.801	0.64
P3, *GlobRad*	Spring	$2.088 \cdot 10^{-9}$	7.778	–	0.49
	Summer	$2.011 \cdot 10^{-9}$	5.457	–	0.45
	Autumn	$1.688 \cdot 10^{-9}$	2.675	–	0.47
	Winter	$1.801 \cdot 10^{-9}$	4.481	–	0.47
P4, *GlobRad*	Spring	$3.582 \cdot 10^{-9}$	–	–	0.42
	Summer	$4.152 \cdot 10^{-9}$	–	–	0.09
	Autumn	$2.159 \cdot 10^{-9}$	–	–	0.22
	Winter	$2.215 \cdot 10^{-9}$	–	–	0.59

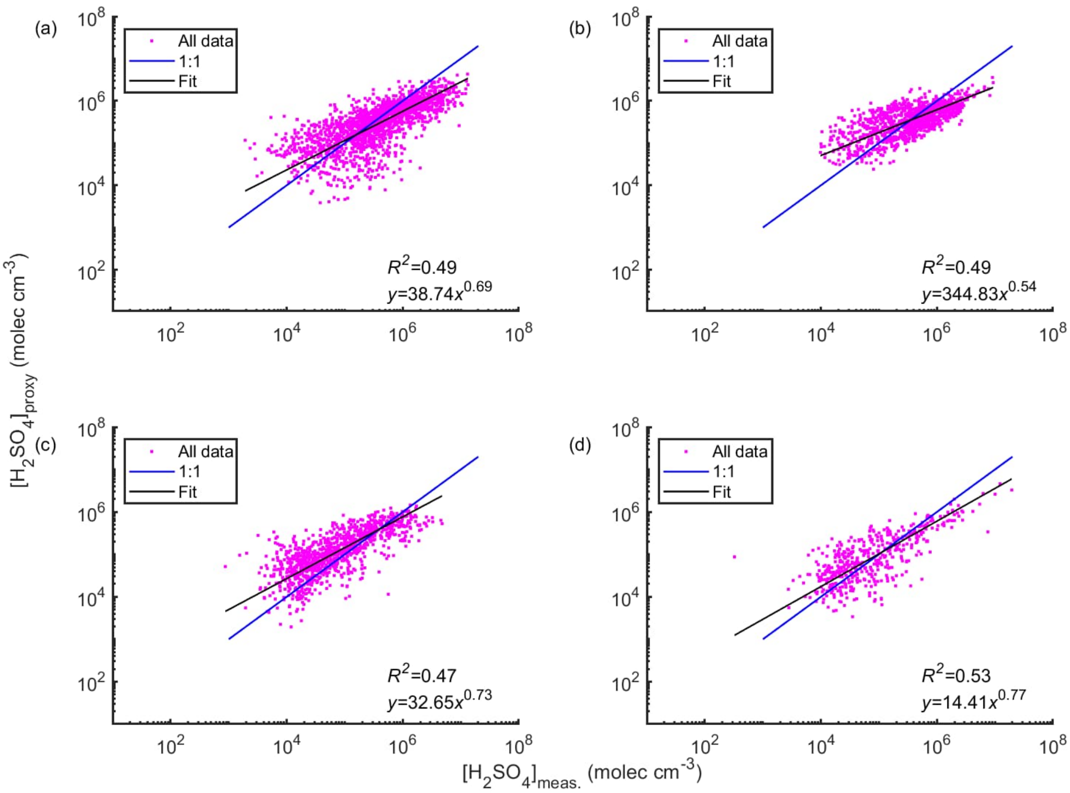

Figure S22: Proxy 1 using global radiation divided seasonally: (a) spring, (b) summer, (c) autumn, and (d) winter.

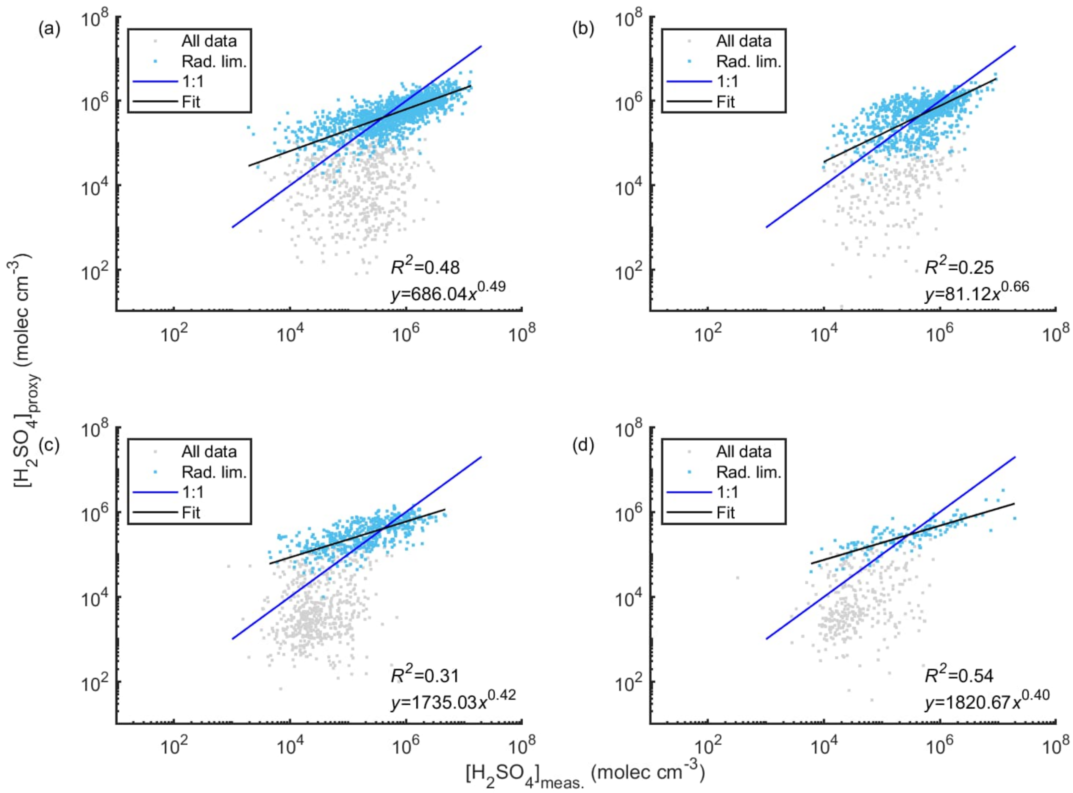

Figure S23: Proxy 2 using UVB radiation divided seasonally: (a) spring, (b) summer, (c) autumn, and (d) winter. We applied radiation limits for the data (colored markers). Without the radiation limits (gray markers), the R^2 values were 0.34, 0.29, 0.42, and 0.40 and fitted lines $y=4\cdot10^{-6}x^{1.91}$, $y=3\cdot10^{-2}x^{1.25}$, $y=6\cdot10^{-6}x^{1.97}$, and $y=2\cdot10^{-6}x^{2.04}$ for spring, summer, autumn, and winter, respectively (fitted lines for all data not shown).

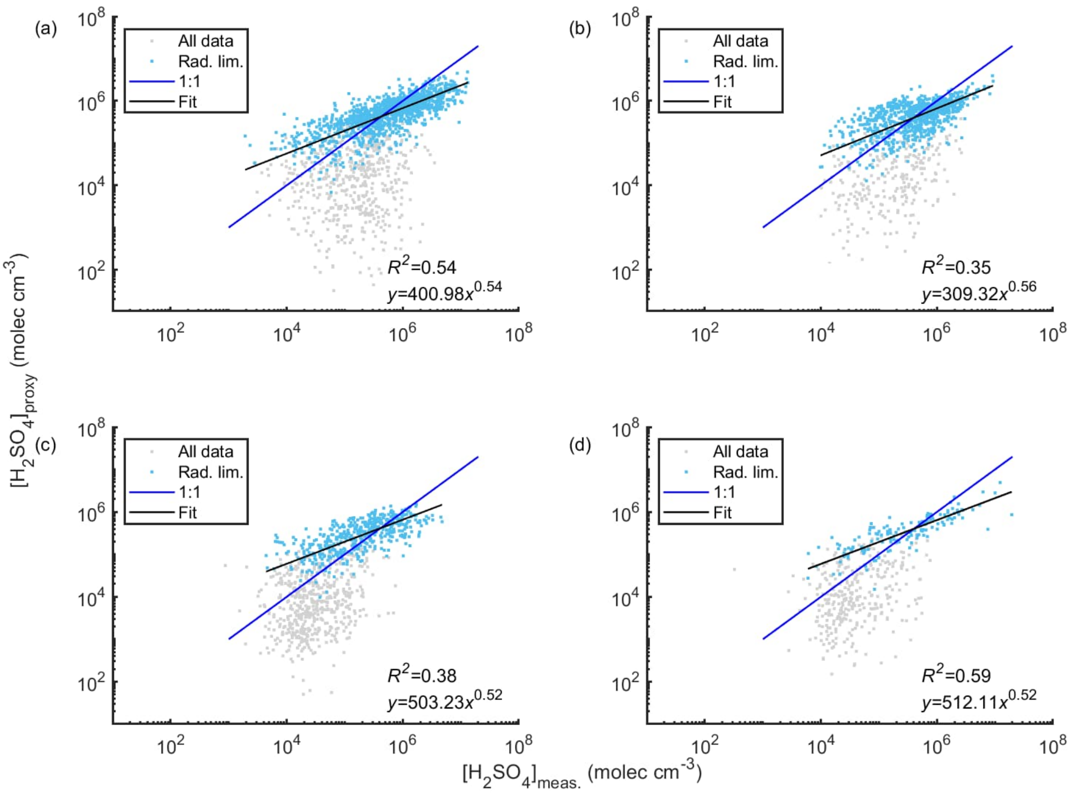

Figure S24: Proxy 2 using global radiation divided seasonally: (a) spring, (b) summer, (c) autumn, and (d) winter. We applied radiation limits for the data (colored markers). Without the radiation limits (gray markers), the R^2 values were 0.34, 0.30, 0.45, and 0.42 and fitted lines $y=3\cdot10^{-5}x^{1.75}$, $y=3\cdot10^{-2}x^{1.24}$, $y=6\cdot10^{-4}x^{1.59}$, and $y=5\cdot10^{-5}x^{1.77}$ for spring, summer, autumn, and winter, respectively (fitted lines for all data not shown).

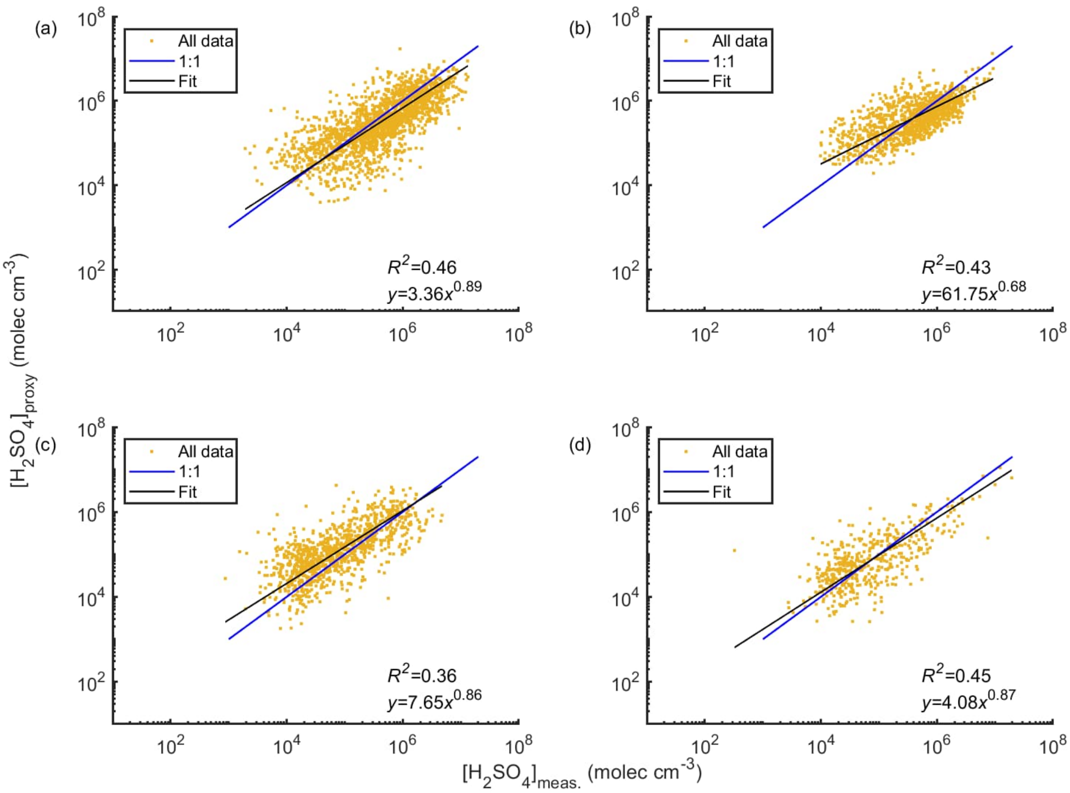

Figure S25: Proxy 3 using UVB radiation divided seasonally: (a) spring, (b) summer, (c) autumn, and (d) winter.

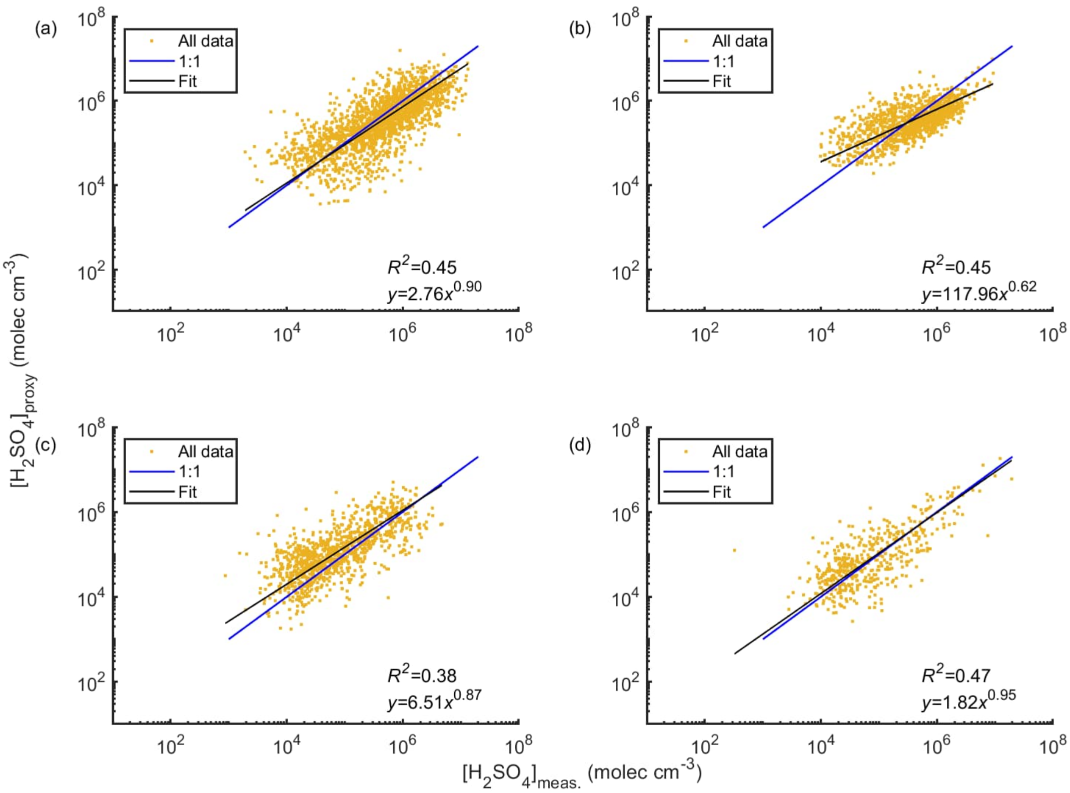

Figure S26: Proxy 3 using global radiation divided seasonally: (a) spring, (b) summer, (c) autumn, and (d) winter.

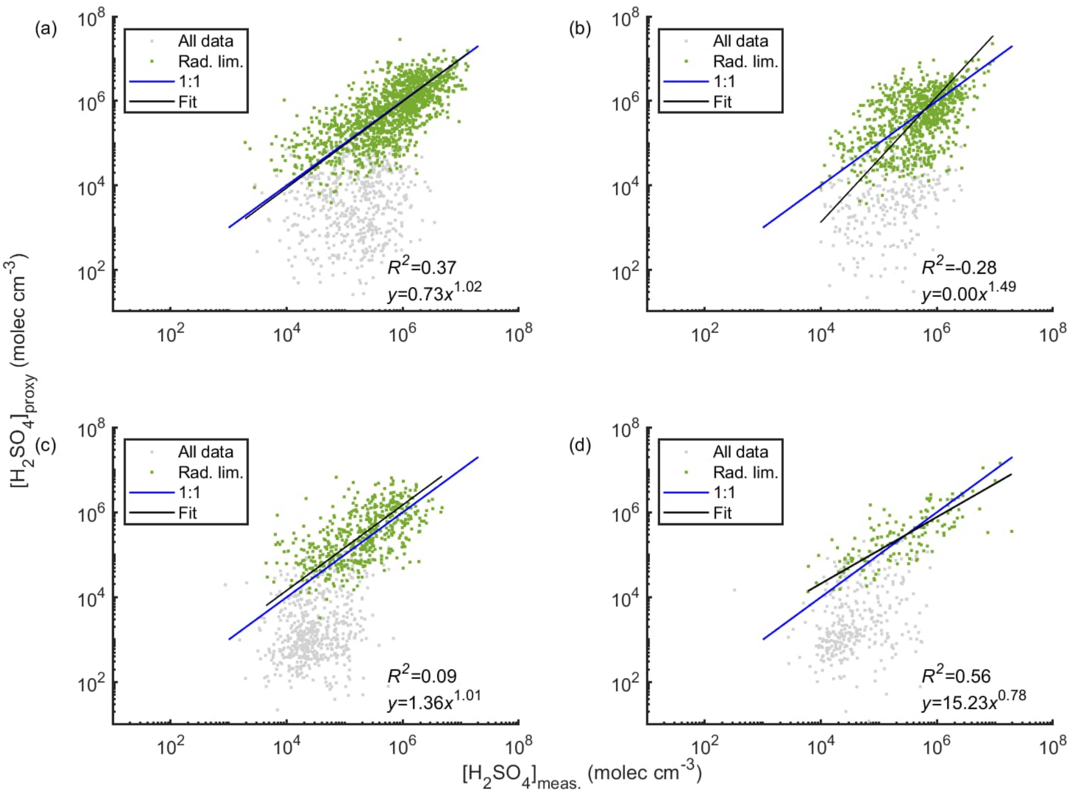

Figure S27: Proxy 4 using UVB radiation divided seasonally: (a) spring, (b) summer, (c) autumn, and (d) winter. We applied radiation limits for the data (colored markers). Without the radiation limits (gray markers), the R^2 values were 0.37, 0.28, 0.45, and 0.41 and fitted lines $y=7\cdot10^{-9}x^{2.38}$, $y=6\cdot10^{-12}x^{2.96}$, $y=7\cdot10^{-9}x^{2.53}$, and $y=2\cdot10^{-7}x^{2.18}$ for spring, summer, autumn, and winter, respectively (fitted lines for all data not shown).

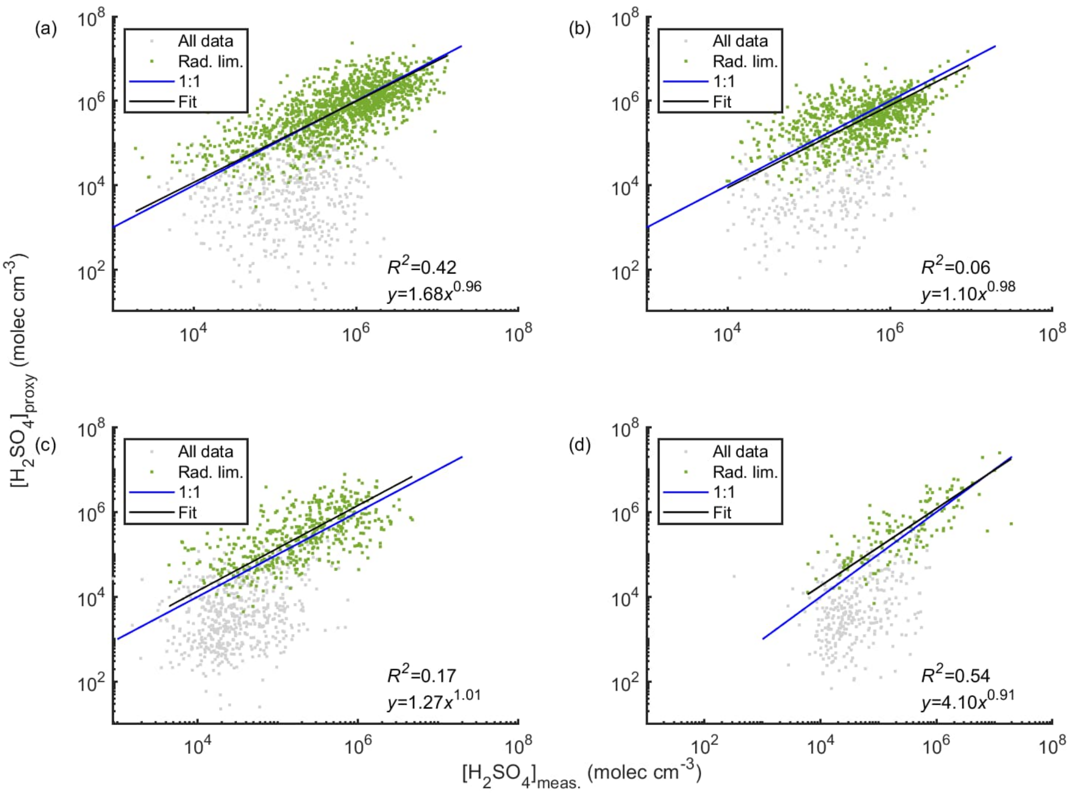

Figure S28: Proxy 4 using global radiation divided seasonally: (a) spring, (b) summer, (c) autumn, and (d) winter. We applied radiation limits for the data (colored markers). Without the radiation limits (gray markers), the R^2 values were 0.37, 0.29, 0.48, and 0.44 and fitted lines $y=1\cdot10^{-7}x^{2.17}$, $y=3\cdot10^{-8}x^{2.30}$, $y=8\cdot10^{-7}x^{2.13}$, and $y=3\cdot10^{-6}x^{1.98}$ for spring, summer, autumn, and winter, respectively.

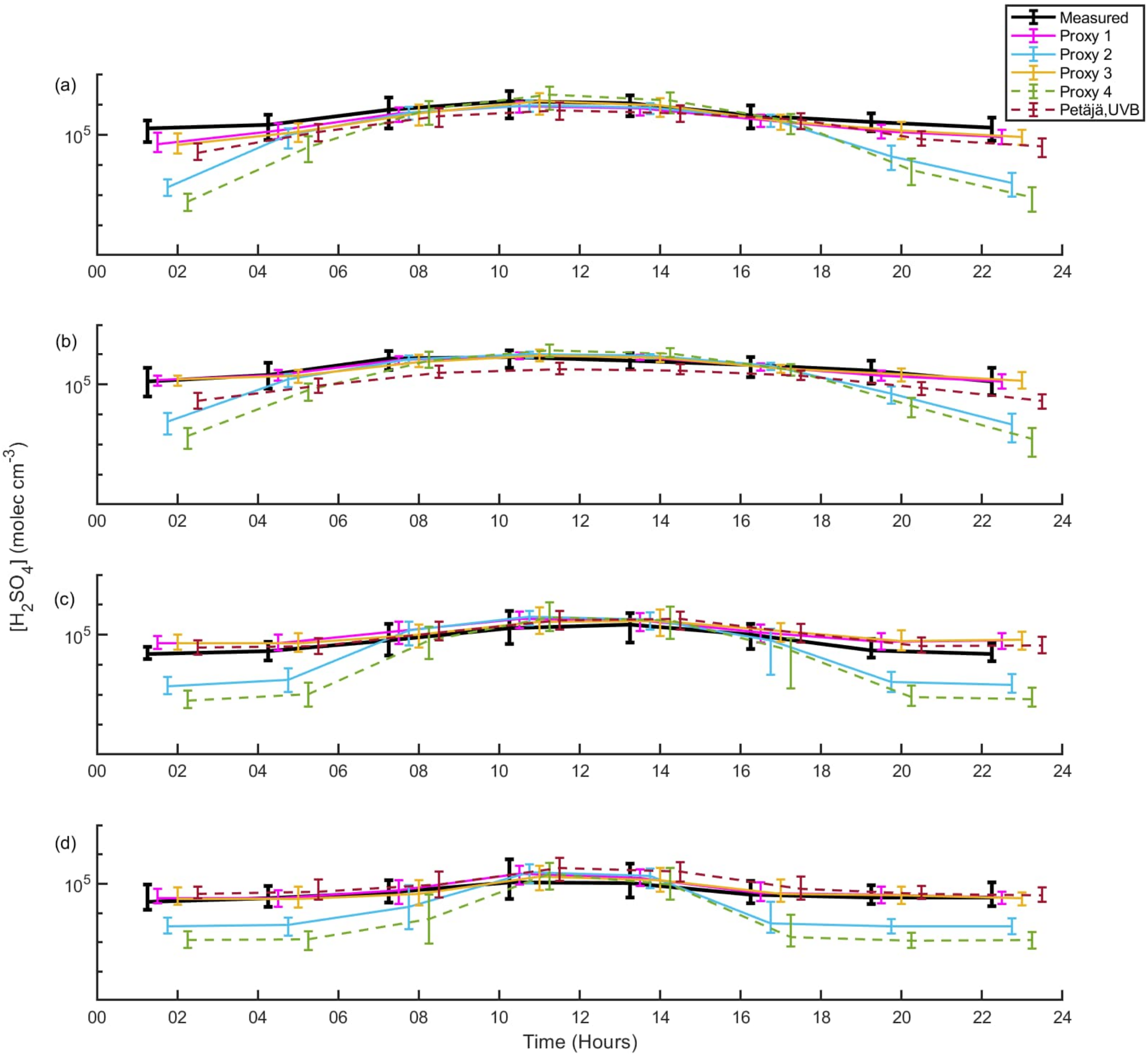

Figure S29: Hourly averaged diurnal variation of sulfuric acid concentration applying different proxies with UVB radiation in (a) spring, (b) summer, (c) autumn, and (d) winter. For further details, see Fig. S19.

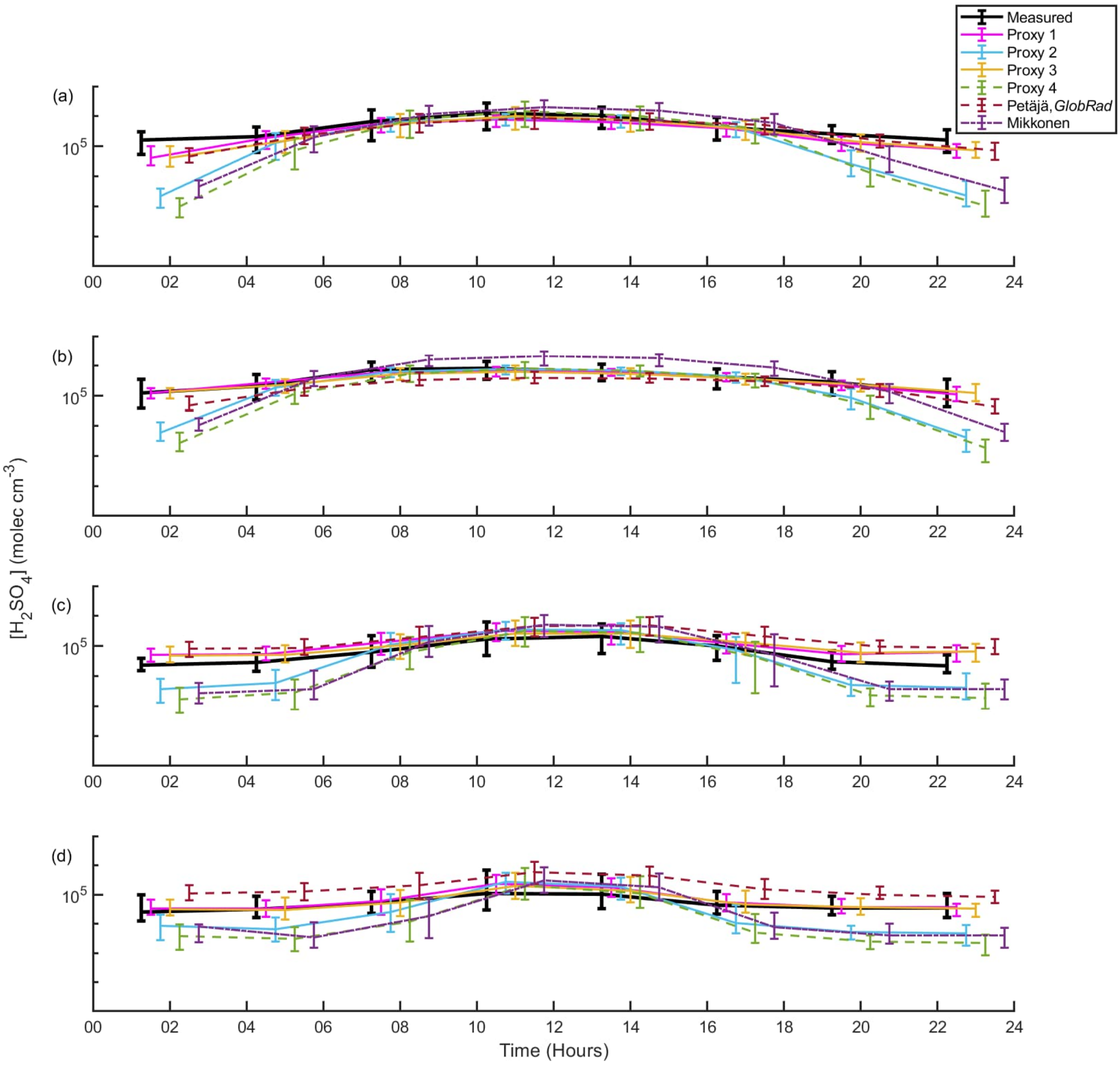

Figure S30: Hourly averaged diurnal variation of sulfuric acid concentration applying different proxies with global radiation in (a) spring, (b) summer, (c) autumn, and (d) winter. For further details, see Fig. S19.

References

Dada, L., Ylivinkka, I., Baalbaki, R., Li, C., Guo, Y., Yan, C., Yao, L., Sarnela, N., Jokinen, T., Daellenbach, K. R., Yin, R., Deng, C., Chu, B., Nieminen, T., Wang, Y., Lin, Z., Thakur, R. C., Kontkanen, J., Stolzenburg, D., Sipilä, M., Hussein, T., Paasonen, P., Bianchi, F., Salma, I., Weidinger, T., Pikridas, M., Sciare, J., Jiang, J., Liu, Y., Petäjä, T., Kerminen, V.-M., and Kulmala, M. 2020. Sources and sinks driving sulfuric acid concentrations in contrasting environments: implications on proxy calculations. Atmospheric Chemistry and Physics, 20(20):11747–11766.

Mikkonen, S., Romakkaniemi, S., Smith, J. N., Korhonen, H., Petäjä, T., Plass-Duelmer, C., Boy, M., McMurry, P. H., Lehtinen, K. E. J., Joutsensaari, J., Hamed, A., Mauldin III, R. L., Birmili, W., Spindler, G., Arnold, F., Kulmala, M. & Laaksonen, A. 2011. A statistical proxy for sulphuric acid concentration. Atmospheric Chemistry and Physics, 11(21):11319–11334.

Petäjä, T., Mauldin III, R., Kosciuch, E., McGrath, J., Nieminen, T., Paasonen, P., Boy, M., Adamov, A., Kotiaho, T. & Kulmala, M. 2009. Sulfuric acid and OH concentrations in a boreal forest site. Atmospheric Chemistry and Physics, 9(19):7435–7448.